

1  
2  
3  
4  
5  
6  
7  
8  
9  
10  
11  
12  
13  
14  
15  
16  
17  
18  
19  
20  
21  
22  
23  
24  
25

## Long-term experimental evolution decouples size and production costs in *Escherichia coli*

Dustin J. Marshall<sup>a,\*</sup>, Martino Malerba<sup>b</sup>, Thomas Lines<sup>a,c</sup>, Aysha L. Sezmis<sup>a</sup>,  
Chowdhury M. Hasan<sup>a</sup>, Richard E. Lenski<sup>d,e</sup>, Michael J. McDonald<sup>a</sup>

<sup>a</sup>Centre for Geometric Biology, School of Biological Sciences, Monash University, Melbourne, Australia; <sup>b</sup>Centre for Integrative Ecology, School of Life and Environmental Sciences, Deakin University, Melbourne, Australia; <sup>c</sup>School of Agriculture, Food and Wine, University of Adelaide, Adelaide, Australia; <sup>d</sup>Department of Microbiology and Molecular Genetics, Michigan State University, East Lansing, MI 48824; <sup>e</sup>Program in Ecology, Evolution, and Behavior, Michigan State University, East Lansing, MI 48824

\*Corresponding author: Dustin J. Marshall

**Email:** dustin.marshall@monash.edu

**Author contributions:** D.J.M., M.M., R.E.L., and M.J.M. designed research; M.M., T.L., A.L.S., C.M.H., and M.J.M. performed research; D.J.M., M.M., and M.J.M. analyzed data; and D.J.M., M.M., R.E.L., and M.J.M. wrote the paper.

**Competing Interest Statement:** The authors declare no conflict of interest.

**Classification:** Evolution.

**Keywords:** biological productivity | body size | metabolic scaling | population dynamics

**This PDF file includes:**

Main Text  
Figures 1 to 3  
Table 1

26 **Abstract**

27 Body size covaries with population dynamics across life's domains. Metabolism may impose  
28 fundamental constraints on the coevolution of size and demography, but experimental tests of  
29 the causal links remain elusive. We leverage a 60,000-generation experiment in which  
30 *Escherichia coli* populations evolved larger cells to examine intraspecific metabolic scaling and  
31 correlations with demographic parameters. Over the course of their evolution, the cells have  
32 roughly doubled in size relative to their ancestors. These larger cells have metabolic rates that  
33 are absolutely higher, but relative to their size, they are lower. Metabolic theory successfully  
34 predicted the relations between size, metabolism, and maximum population density, including  
35 support for Damuth's law of energy equivalence, such that populations of larger cells achieved  
36 lower maximum densities but higher maximum biomasses than populations of smaller cells. The  
37 scaling of metabolism with cell size thus predicted the scaling of size with maximum population  
38 density. In stark contrast to standard theory, however, populations of larger cells grew faster  
39 than those of smaller cells, contradicting the fundamental and intuitive assumption that the costs  
40 of building new individuals should scale directly with their size. The finding that the costs of  
41 production can be decoupled from size necessitates a reevaluation of the evolutionary drivers  
42 and ecological consequences of biological size more generally.

43 **Significance statement**

44 Populations of larger organisms should be more efficient in their resource use, but grow more  
45 slowly, than populations of smaller organisms. The relations between size, metabolism, and  
46 demography form the bedrock of metabolic theory, but most empirical tests have been  
47 correlative and indirect. Experimental lineages of *E. coli* that evolved to make larger cells  
48 provide a unique opportunity to test how size, metabolism, and demography covary. Despite the  
49 larger cells having a relatively slower metabolism, they grow faster than smaller cells. They  
50 achieve this growth-rate advantage by reducing the relative costs of producing their larger cells.  
51 That evolution can decouple the costs of production from size challenges a fundamental  
52 assumption about the connections between physiology and ecology.

53

54 **Main Text**

55 **Introduction**

56 Differences in the sizes of individual organisms drive widespread and repeated patterns across  
57 the tree of life (1-4). For example, Damuth's Rule holds that larger organisms have lower  
58 population densities than smaller organisms (5). Similarly, populations of larger organisms grow  
59 more slowly than populations of smaller organisms (6). Meanwhile, global warming and  
60 harvesting are causing declines in body size in many species, from phytoplankton to fish (7-10).  
61 If body size and demography covary within species as they do across species, then human-  
62 induced changes in body size may have important consequences for ecosystem function,  
63 particularly with regards to food security and the global carbon pump (11). However, our ability  
64 to anticipate such changes is limited by the dearth of studies examining the within-species  
65 covariance of size, energy, and demography.

66 Metabolism has long been argued to provide the mechanistic link between size and  
67 demography because it governs the rate at which organisms transform energy into biological  
68 work and growth (4-6). Larger-sized species have higher absolute metabolic rates than smaller  
69 species, but lower metabolic rates relative to their size. In formal terms, absolute metabolism  
70 scales hypoallometrically with body size with an exponent of  $B$ , whereas mass-specific  
71 metabolism scales at  $B - 1$ . The hypoallometric scaling of size and metabolism generates  
72 several predictions for how size should affect demography (12).

73 First, because the ability to perform biological work per unit mass should scale with mass-  
74 specific metabolic rates, maximum rates of population growth ( $r$ ) should scale at  $B - 1$  (refs. 6,  
75 12). For metazoans,  $B$  is typically  $\sim 0.75$ ; thus,  $r$  should scale around  $-0.25$ , which is strongly  
76 supported by interspecific comparisons (4). This prediction has intuitive appeal: mouse  
77 populations can grow much faster than elephant populations.

78 Second, smaller species should attain higher maximum population densities ( $K$ ) than larger  
79 species, because their absolute *per capita* demands are lower. The resource requirements of  
80 organisms depend on their metabolism, so populations of larger species should cease growing  
81 at lower densities than those of smaller species (5). However, larger organisms have lower  
82 mass-specific metabolic rates (in metazoans, at least), and so they require fewer resources per  
83 unit mass than smaller organisms. Accordingly, populations of larger organisms should have  
84 greater total mass at carrying capacity than populations of smaller organisms, with the expected  
85 scaling at  $1 - B$  (ref. 1). This relation is known as the theory of energy equivalence (3).

86 Finally, the maximum rate of population productivity (effectively the product of  $r$  and  $K$ ) should  
87 scale with size at  $-1$  when expressed as the rate of production of individuals, and so it should  
88 be size-independent (i.e., scaling exponent of 0) in terms of the rate of biomass production (2,  
89 12). Together these three predictions represent the canonical elements of how size,  
90 metabolism, and energy equivalence determine population growth and dynamics. Put simply,  
91 populations of larger organisms, with lower mass-specific metabolic rates, should grow more  
92 slowly, but eventually achieve higher total biomass, than populations of smaller organisms (4).  
93 Nonetheless, there remains a fundamental disconnect between theory and evidence: most tests  
94 are based on among-species comparisons, making it difficult to attribute metabolism as the  
95 underlying driver of such patterns.

96 Although metabolic theory successfully predicts variation in demography across the domains of  
97 life, these predictions often falter when applied to narrower taxonomic groups (2, 12-14).  
98 Various explanations have been offered for these discrepancies, but a key difficulty lies in  
99 inferring causality with respect to size differences across species. Mice differ from elephants in  
100 ways other than size, but metabolic theories about the relation between size and demography  
101 ignore these differences, treating them as an error term that is uncorrelated with size. We know,  
102 however, that many other traits covary with size (e.g., lifespan generally increases with size),  
103 and these traits also affect population dynamics (4, 6). Interspecific comparisons of individual  
104 size and population dynamics therefore confound other species-specific traits that influence  
105 demographic variables. Consequently, it remains unclear whether size, energy, and population  
106 dynamics are invariably related as supposed by the canonical scaling theory. Meanwhile, our  
107 capacity to predict the consequences of human-mediated impacts on the size of organisms  
108 depends on understanding the causal links between these factors within species.

109 Intraspecific tests of the relation between body size and demography are challenging.  
110 Comparisons among individuals of the same species suffer from limited power because they  
111 compare a narrower range of sizes than comparisons across species. Intraspecific comparisons  
112 of individuals at different ontogenetic stages can span a greater size range, but this approach  
113 also introduces confounding factors and cannot be extended to demographic parameters that  
114 must integrate across all ontogenetic stages. Ideally, a species that varies significantly in size  
115 across populations, and that allows the direct parameterization of population dynamical models,  
116 would provide valuable evidence of how intraspecific variation in size and metabolic rates  
117 affects demography. However, such tests are rare (2, 11), and they have typically relied on

118 either temperature manipulation or strong artificial selection for individual size to generate  
119 differences.

120 Here we analyze the relations among organismal size, metabolism, and demography in 12  
121 populations of *Escherichia coli* that have evolved and diverged from a common ancestor in the  
122 Long-Term Evolution Experiment (LTEE) for more than 60,000 generations (15). The  
123 populations are diluted 100-fold in fresh culture medium each day. They undergo ~6.7  
124 generations (cell doublings) before they exhaust the limiting resource, which is glucose. The  
125 bacteria thus experience alternating periods of growth and stationary phase, while the  
126 composition of the medium and other aspects of their environment are kept constant. The LTEE  
127 populations have been extensively characterized, including by competitive fitness assays as  
128 well as whole-genome and whole-population sequencing (16-18). Over the duration of the  
129 LTEE, each population has steadily increased in fitness, while accumulating many mutations.  
130 The average size of individual cells also increased during the LTEE (19-21). The LTEE imposes  
131 no direct, artificial selection on cell size or any other individual phenotypic trait. Instead, the  
132 changes in size evolve incidentally, as correlated responses to selection favoring faster growth  
133 (22). In this study, we measure the population dynamics, metabolism, and cell size of the  
134 ancestral and evolved bacteria to determine how these factors covary, thereby allowing us to  
135 test whether they conform to predictions based on standard metabolic theory. In particular, we  
136 examine population growth rates and yields and find that the evolution of larger cell sizes has  
137 led to 'Pareto improvements' whereby growth rate has increased but not at the expense of yield  
138 (23, 24).

## 139 **Results**

140 We examined two clones from each of the 12 LTEE populations at the 10,000 and 60,000  
141 generation time points. We excluded the 60,000-generation clones from one population (Ara-3)  
142 that evolved the ability to consume citrate (25), which is present in the medium as a chelating  
143 agent, because it gives cells access to an additional resource that confounds the relation  
144 between metabolism and demography that we seek to understand. The fundamental unit of  
145 independent replication in the LTEE, and in evolution experiments generally, is the evolving  
146 population, and not the individual (15-19). Therefore, in all analyses, we treat the average value  
147 of the two clones from the same population and generation as a single sample. We also include  
148 the two ancestral strains, REL606 and REL607, each of which was used to found six  
149 populations, and which differ by a genetic marker used in competition assays (15, 16, 19). Thus,

150 our analyses include a total of 25 samples (2 ancestors, 12 populations at 10,000 generations,  
151 and 11 populations at 60,000 generations).

152 Previous studies reported large increases in cell volume in the first 50,000 generations of the  
153 LTEE (19-21). Our measurements confirm the large increases in cell size and show that they  
154 have continued to increase, from an average of 0.239 fL (i.e.,  $\mu\text{m}^3$ ) for the ancestors to an  
155 average of 0.670 fL for the 60,000-generation samples (Fig. 1). The evolving populations  
156 followed different size trajectories, but they all show the same trend of increasing size.

157 We quantified metabolism by measuring oxygen consumption at three initial cell densities,  
158 achieved by differentially diluting samples. The concentration of the limiting resource, glucose,  
159 was the same for all three initial densities, and it was insufficient to support one population  
160 doubling even at the lowest initial density. As a result, the glucose was depleted over the course  
161 of our measurements of oxygen consumption, leading to a transition into stationary phase and  
162 concomitant decline in the *per capita* respiration rates at the higher initial densities. At all three  
163 initial cell densities, metabolism scaled with average cell size (volume) sub-linearly (Fig. 2), and  
164 the scaling relation was consistent across the densities (Density x log[Cell size]:  $F_{2,69} = 0.082$ ,  $P$   
165 = 0.921; Density:  $F_{2,71} = 97.06$ ,  $P < 0.0001$ ; log[Cell size]:  $F_{1,71} = 45.99$ ,  $P < 0.0001$ ). The  
166 estimated scaling exponent for the metabolic rate,  $B$ , is 0.38, which differs significantly from  
167 interspecies comparisons (26) that have estimated the scaling exponent to be  $>1$ , and from  
168 theoretical expectations based on surface-area-to-volume ratios of  $\sim 0.67 - 1$  (depending on cell  
169 shape). With our empirical estimate of the intraspecific metabolic scaling exponent, we can then  
170 use standard metabolic theory to predict how population growth rates and maximum population  
171 size should scale with cell size (Table 1).

172 We measured population growth over 24 h for all the samples, each at three different resource  
173 levels achieved by varying the concentration of glucose in the medium, and with replication of  
174 the growth curves at each concentration. Populations grew slightly faster at the higher glucose  
175 concentrations (Fig. 3a). However, the scaling of the maximum growth rate,  $r$ , was consistent  
176 across glucose levels (Glucose x log[Cell size]:  $F_{2,69} = 0.113$ ,  $P = 0.893$ ). The scaling exponent  
177 of the growth rate was 0.27, which differs significantly from both zero and the exponent ( $-0.63$ )  
178 predicted by the canonical theory (Table 1). Instead, the scaling of the growth rate is much  
179 closer to that of the metabolic scaling (0.38 versus 0.27).

180 The maximum yield in terms of cell density ( $Max_{cells}$ ) showed a negative scaling relation with cell  
181 volume, with an exponent of  $-0.45$  (Fig. 3b), and the confidence interval overlaps the prediction

182 of  $-0.38$  from theory (Table 1). The correlation between cell size and maximum cell density was  
183 strong; a model including glucose level and cell size explained 96% of the variation in maximum  
184 cell density. The maximum biovolume yield ( $Max_{biovolume}$ ) scaled positively with cell size with an  
185 exponent of 0.55 (Fig. 3c), again in reasonable agreement with the theoretical expectation of  
186 0.64 (Table 1). As expected, populations achieved higher biovolumes at higher glucose levels  
187 (Fig. 3c), but the scaling relation was again consistent across the three glucose levels (glucose:  
188  $F_{2,71} = 437.32$ ,  $P < 0.0001$ ; glucose x log[cell size]:  $F_{2,69} = 0.257$ ,  $P = 0.774$ ).

189 Maximum productivity, expressed as the maximum rate of biovolume increase, increased with  
190 average cell size (Fig. 3d), with an estimated exponent of 0.81 (Table 1). This estimate differs  
191 greatly, and significantly, from the canonical expectation of zero (Productivity<sub>biovolume</sub>:  $F_{1,71} =$   
192  $301.5$ ,  $P < 0.0001$ ). Productivity increased at higher glucose levels (glucose:  $F_{2,71} = 410.5$ ,  $P$   
193  $< 0.0001$ ), with no significant interaction between cell size and glucose levels ( $F_{2,69} = 0.447$ ,  $P =$   
194  $0.641$ ).

195 Table 1 summarizes our empirical results relative to theoretical expectations. The scaling of  
196 maximum population size with individual size was similar to the predictions made by metabolic  
197 theory, regardless of whether it was measured in terms of cell number (Fig. 3b) or total  
198 biovolume (Fig. 3c). In contrast, productivity did not conform to the predictions made by the  
199 canonical metabolic theory, whether measured as the rate of population increase (Fig. 3a) or  
200 the maximum biovolume productivity (Fig. 3d). Instead, both productivity exponents were much  
201 higher than the canonical theory would predict, by values of 0.89 and 0.81, respectively.

## 202 **Discussion**

203 The LTEE provides a unique opportunity to study the covariance between size, metabolism, and  
204 demography within a species. Damuth's law of energy equivalence successfully predicted the  
205 coevolution of individual cell size with maximum population density (5). However, we also  
206 discovered that a fundamental assumption about how the growth and productivity of populations  
207 should scale with metabolism and size lacks generality and therefore requires modification. Our  
208 study shows the value of, and need for more, within-species tests of metabolic theory. Of  
209 particular interest, our results indicate that evolution sometimes produces Pareto improvements  
210 in key size-related parameters—leading to trade-ups, rather than trade-offs—that are not  
211 anticipated from interspecific comparisons among both multicellular (6) and unicellular  
212 organisms (27, 28).

213 **Larger Cells Have Relatively Lower Metabolic Rates than Smaller Cells.** The scaling of  
214 metabolic rate with size in these experimental *E. coli* populations is remarkably low, with an  
215 exponent of only ~0.38. Among-species comparisons of metabolic rate in bacteria have usually  
216 reported hyperallometric scaling ( $B > 1$ ), whereby larger cells have disproportionately higher  
217 metabolic rates (26, 29). By contrast, we find that the larger cells from later generations of the  
218 LTEE have much lower mass-specific metabolic rates than their smaller ancestors, such that a  
219 doubling in size leads to only a 30% increase in metabolism.

220 There are several potential explanations for the low scaling exponent that we observe in this  
221 experiment relative to interspecific comparisons. First, it could be that within-species metabolic  
222 scaling is generally shallower than interspecific scaling in bacteria; to date, there are too few  
223 studies that have measured within-species scaling to compare them. In other taxa, metabolic  
224 scaling sometimes differs depending on whether it is estimated within or among species (30,  
225 31). Theory predicts that, all else equal, the physics of resource limitation in slow-moving fluids  
226 should result in metabolic scaling exponents of about 0.33 (ref. 32), which is close to our  
227 estimate. The cytoplasm of bacterial cells is viscous and densely packed with DNA and other  
228 macromolecules (20, 21). It could also be that physical constraints on scaling are more  
229 restrictive within than among species. For example, cell shape may change with cell size more  
230 substantially among species than within species (32). It should be noted, however, that the  
231 aspect ratio (length/width) also varies significantly among the *E. coli* lineages in this study (21).

232 Second, the fine-tuning of gene regulation and physiological process may have produced the  
233 low metabolic scaling exponents seen in the LTEE. DeLong et al. (26) suggested that  
234 hyperallometric metabolic scaling in bacteria emerges from the effect of genome size on  
235 metabolic rate. Larger cells typically have larger genomes; more genes and gene products  
236 might drive higher metabolic rates (33). Although the average haploid genome length has  
237 declined slightly during the LTEE owing to some gene deletions (17), rapidly growing bacterial  
238 cells typically have multiple copies of their chromosome. Therefore, the faster-growing and  
239 larger evolved bacteria have more total DNA per cell, even if their genome length is slightly  
240 smaller. Among prokaryotes, genome length scales with cell size with an exponent of 0.35 (ref.  
241 26), which is close to the 0.38 metabolic exponent we observed (Fig. 2, Table 1). The bacteria  
242 in the LTEE have evolved substantial changes in gene expression and regulation (34-36).  
243 These changes have reduced the expression of functions that are no longer useful in the  
244 LTEE's simple conditions, while optimizing the expression of the functions that are still needed  
245 (37). Such changes may be especially important in an environment that varies cyclically

246 between resource abundance and depletion in a predictable manner over time, as it does in the  
247 LTEE (15, 34).

248 **Metabolic Theory Predicts Maximum Population Size.** We found strong support for the  
249 energy equivalence rule across a range of resource levels (5). Because the mass-specific  
250 metabolic rates of the larger evolved cells were so low, the maximum biovolume yields were  
251 much higher in those samples than in the ancestors (Fig. 3c). However, the total metabolic  
252 demands of these two groups were similar ( $\sim 4.5 \times 10^{-3}$  J). Thus, the larger cells are  
253 metabolically more efficient and attain higher population biomass than smaller cells from a given  
254 amount of resource. This result conforms with other LTEE studies that found that the evolved  
255 cells are larger, more efficient, and attain higher maximum biomass yields than the ancestors  
256 (20, 23). It seems that metabolic rate can be an excellent predictor of the limits to population  
257 biomass, both among (4) and within species (11). In contrast, longstanding metabolic theories,  
258 based on standard assumptions, failed to predict how individual size and metabolism would  
259 impact population growth rates and maximum productivity.

260 **Metabolic Theory Does Not Predict Population Growth Rates.** The *E. coli* samples in this  
261 study defy theoretical predictions based on standard assumptions about how individual size  
262 should affect rates of population growth and production. Despite having lower mass-specific  
263 metabolic rates, the larger evolved cells have higher intrinsic rates of increase ( $r$ ) than the  
264 smaller ancestral cells. One might expect that larger cells would require more materials and  
265 energy to produce, but relative to their volume, they would also have less capacity to power this  
266 work than smaller cells. Nonetheless, our study, other studies of the LTEE populations, and  
267 indeed studies on *E. coli* more generally find that faster growing cells are larger than cells  
268 growing more slowly (20, 23, 38, 39). This positive correlation between size and growth rate  
269 contradicts the expectation based on standard theory.

270 Standard theory predicts that population growth rate should scale with the mass-specific  
271 metabolic rate (i.e.,  $M^{B-1}$ ) (refs. 6, 12, 40). This theory works well for among-species  
272 comparisons: in multicellular eukaryotes, both mass-specific metabolic rate and population  
273 growth rate scale at  $\sim M^{-0.25}$  (refs. 1, 4); and in prokaryotes, both rates appear to scale at  $\sim 1$   
274 (refs. 26, 41). However, in the *E. coli* from the LTEE, population growth rate scales at 0.27, an  
275 exponent that is 0.89 higher than expected given the mass-specific scaling of  $-0.62$ . In fact, the  
276 population growth rate exponent is much closer to the *per capita* metabolic exponent of 0.38  
277 than to the mass-specific exponent of  $-0.62$ . Why do these bacteria show positive scaling of

278 both *per capita* metabolism and population growth rate with individual size, contradicting  
279 expectations based on the standard theory?

280 **Metabolic Theory and the Costs of Biological Production.** A crucial, but often overlooked,  
281 assumption of standard metabolic theory is that the energy required to produce a new individual  
282 is directly proportional to its mass (6). This assumption seems reasonable at first glance, but in  
283 fact there is little empirical evidence to support it and, in the case of the LTEE, some evidence  
284 against it. The total cost of producing a cell is the sum of the energy consumed between cell  
285 divisions (sometimes called maintenance costs) and the energy used to build the new cell itself  
286 (41). Neither component is likely to scale directly with cell volume, for several reasons.

287 First, it has been estimated that about half of the energy required by *E. coli* is used to maintain  
288 ion gradients across the cell membranes (42). Larger cells have smaller surface area relative to  
289 mass, and so they should have relatively lower maintenance costs than smaller cells.  
290 Consistent with this reasoning, total metabolism scales hypoallometrically with cell volume in the  
291 LTEE. Second, large cells often have different stoichiometry from small cells. Both among and  
292 within taxa, large cells tend to have relatively lower carbon content than small ones (43). In the  
293 LTEE specifically, size and carbon density do not scale proportionately, and the stoichiometry of  
294 cells has evolved over time (20, 44). In this light, the assumption of equal costs per unit volume  
295 of building smaller and larger cells is violated. Finally, large cells are relatively cheaper to  
296 produce than small cells in terms of genome replication. In the LTEE, the larger evolved cells  
297 have slightly smaller genomes than the smaller ancestral cells (17), so that the relative, and  
298 even absolute, costs of genome replication are lower for the larger cells. Of likely greater  
299 importance, the evolved cells have undergone substantial fine-tuning of their gene-regulatory  
300 networks to the LTEE environment, thus reducing the costly expression of unneeded transcripts  
301 and proteins (34-37).

302 **Relaxing the Strict Proportionality of Production Costs and Size.** Taken together, our  
303 results imply that larger cells are cheaper to maintain and build per unit volume, such that the  
304 scaling of the total cost of production is far less than proportional to cell size. If the assumption  
305 of proportional cost is relaxed, then the paradox of larger cells having higher growth rates may  
306 be resolved. Instead of assuming that the costs of production scale with individual cell size with  
307 an exponent of 1, we can explore a range of possible scaling exponents and compare the  
308 resulting predictions with our observations. To that end, here is the generalized formula relating  
309 cell size to population growth rate:

$$r = M^B/M^C \quad (\text{Eq. 1})$$

310 where  $B$  is the exponent linking cell mass to metabolic rate, and  $C$  is the exponent linking total  
311 production costs (both maintenance and building) to mass. When the costs are assumed to be  
312 directly proportional to size (i.e.,  $C = 1$ ), we recover the prediction of classic metabolic theory  
313 (6):

$$r = M^B/M^1 = M^{B-1} \quad (\text{Eq. 2})$$

314 At the other extreme, the costs of production are size invariant (i.e.,  $C = 0$ ). That is, the total  
315 costs of producing smaller and larger cells are the same, and theory would instead predict:

$$r = M^B/M^0 = M^B \quad (\text{Eq. 3})$$

316 Of course, any value of  $C$  is possible in this more general framework. In the case of the LTEE  
317 strains, we find that  $r$  scales at 0.27, which implies that  $C = 0.11$  (i.e.,  $0.38 - 0.27 = 0.11$ ). In  
318 other words, the costs increase only weakly with cell size. Specifically, the cells from generation  
319 60,000 are, on average, roughly twice the volume of their ancestors (Fig. 1), but each one costs  
320 only ~10% more to produce than a small ancestral cell. If we now set the exponent that links  
321 production cost ( $C$ ) to size at 0.11, then we can predict much more accurately the scaling  
322 exponent for the maximum rate of biovolume production seen in our experiments (Table 1). In  
323 other words, if we assume the *per capita* cost of producing the larger evolved cells is only  
324 slightly more than the cost of the smaller ancestral cells, then we can reconcile our other  
325 observations with the classic theoretical predictions.

326 A recent study of the single-celled eukaryote *Dunaliella tertiolecta* also found improvements in  
327 both population growth rate and yield as cells evolved to be larger (2). These improvements  
328 were associated with the evolution of significant genomic streamlining (45), which likely  
329 decoupled some production costs from cell size. Thus, it seems that the trade-offs between size  
330 and rates of production that seem almost invariant in comparisons among species can, at least  
331 sometimes, be circumvented within species when other traits that affect metabolic costs also  
332 coevolve. Whether the same decoupling of size and production costs can occur in metazoans,  
333 with their complex development and life cycles, is unclear and, in our view, deserves attention.

334 In conclusion, our results demonstrate the importance of examining the scaling of size,  
335 metabolism, and population dynamics within species, as well as across species, because these  
336 comparisons may differ quantitatively and even qualitatively. Such differences can occur even  
337 though the explanations for these patterns at both scales involve the same underlying metabolic  
338 processes. Given the importance of the scaling of production costs to organismal size in driving

339 our expectations of how size affects population growth and productivity (4), this issue has  
340 received far too little empirical attention. We recommend, therefore, that future studies examine  
341 production costs as a function of size, both within and among species.

## 342 **Materials and Methods**

343 **Experimental Overview.** We measured average cell volumes for 48 *E. coli* clones: 2 ancestral  
344 strains, 2 clones sampled from each of the 12 LTEE populations at 10,000 generations, and 2  
345 clones from 11 of those populations at 60,000 generations (Table S1). We excluded from our  
346 analyses one population at 60,000 generations because it evolved the ability to use citrate as an  
347 additional source of carbon and energy in the LTEE environment. We measured metabolic rates  
348 of the same 48 clones at 3 initial cell densities. We monitored the population growth of the 48  
349 clones at each of 3 resource levels, to which we fit growth curves. The key unit of independent  
350 replication in the LTEE, and in evolution experiments generally, is the evolving population, not  
351 the individual organism (15-19). Thus, we averaged the estimates of cell size, metabolic rate,  
352 and population growth parameters for the two evolved clones from the same population and  
353 generation, and we treat that average value as a single sample. We also include the two  
354 ancestral strains, each of which founded six of the LTEE populations. Thus, our statistical  
355 analyses reflect a total of 25 samples (2 ancestors, 12 populations at 10,000 generations, and  
356 11 populations at 60,000 generations) for each assay and, when relevant, for each treatment.

357 **Evolution Experiment, Strains, and Media.** The LTEE started in 1988 (15), and it has  
358 continued since. Twelve 50-mL flasks containing 10 mL of DM25 medium (see recipe below)  
359 were seeded with either the arabinose-negative ancestral strain REL606 (populations Ara-1 to  
360 Ara-6) or the arabinose-positive ancestor REL607 (populations Ara+1 to Ara+6). The Ara  
361 marker causes cells to produce either red (Ara<sup>-</sup>) or white (Ara<sup>+</sup>) colonies on tetrazolium-  
362 arabinose indicator plates, and it serves to differentiate competitors during relative fitness  
363 assays. The Ara marker is selectively neutral in the LTEE conditions (15, 46, 47). The 12  
364 populations are propagated daily with 100-fold dilutions at 37°C while shaking at 120 rpm for  
365 mixing and aeration. The dilutions and regrowth allow  $\log_2 100 \cong 6.6$  cell generations per day.  
366 The stationary-phase (i.e., end of day) population density is  $\sim 5 \times 10^7$  cells/mL for the ancestral  
367 strains (15). In 11 populations, the stationary-phase population density declined as the  
368 individual cells became larger; in the case of population Ara-3, however, the cell density  
369 increased several-fold after cells evolved the new capacity to use the citrate in DM25 as an  
370 additional source of carbon and energy (25). Samples (including whole populations and isolated

371 clones) are periodically stored with glycerol (as cryoprotectant) at  $-80^{\circ}\text{C}$ , where the cells remain  
372 viable and available for further analyses.

373 As noted above, our analyses used the two ancestors, plus two clones sampled from each  
374 population at 10,000 and 60,000 generations (except for Ara-3 at 60,000 generations, which we  
375 excluded owing to its access to citrate as an additional substrate for growth). The 10,000-  
376 generation clones were isolated and described previously (17). For this study, we plated each  
377 60,000-generation whole-population sample on Lysogeny Broth (LB) agar and picked two  
378 clones at random, which we then stored as glycerol stocks.

379 The culture medium used in the LTEE and in this study is Davis Mingioli (DM) minimal medium  
380 [7 g/L potassium phosphate (dibasic trihydrate), 2 g/L potassium phosphate (monobasic  
381 anhydrous), 1 g/L ammonium sulfate, 0.5 g/L disodium citrate, 1 mL/L 10% magnesium sulfate,  
382 and 1 mL/L 0.2% thiamine (vitamin B1)] supplemented with a specified amount of glucose (15,  
383 46). The concentration of glucose added to the medium is indicated by a suffix (e.g., DM25 has  
384 25 mg/L glucose). MG agar plates were used for counting colonies; in addition to the ingredients  
385 of DM media, MG agar contains 4g/L of glucose and 16g/L agar. LB broth [NaCl (10 g/L),  
386 tryptone (10 g/L), and yeast extract (5 g/L)] was used for the initial recovery of bacteria from  
387 thawed glycerol stocks prior to performing the hemocytometer counts. LB plates were made by  
388 adding 20 g/L agar.

389 **Population Growth Measurements.** Each clone was revived from a frozen stock and then  
390 grown in 3 mL of DM25 at  $37^{\circ}\text{C}$  with orbital shaking for 24 h to acclimate the bacteria to that  
391 medium. The next day, we measured the optical density (OD) of each culture, and the density  
392 was normalized to match the culture with the lowest OD. The resulting cultures were diluted  
393 100-fold into 96-well microplates containing DM25, DM50, or DM100 media. Each clone was  
394 replicated 4 times in each medium, for a total of 600 growth curves (50 clones x 3 media x 4  
395 replicates, including the two clones from population Ara-3 at generation 60,000 that were  
396 subsequently excluded). The clones were randomly assigned to wells for each medium over 20  
397 microplates to minimize position effects. We measured OD at 600 nm wavelength every 10 min  
398 for 24 h using an ELx808 Incubating Absorbance Microplate Reader (BioTek Instruments, USA)  
399 set to its maximum shaking speed and  $37^{\circ}\text{C}$ .

400 A complete description of the methods that we used to estimate demographic parameters is  
401 provided in Malerba et al. (48). Briefly, OD serves as a proxy for population biomass, and we  
402  $\log_e$ -transformed OD values to reduce heteroscedasticity. We then fit the following four-  
403 parameter logistic-type sinusoidal growth model to the data:

$$\log_e OD_{600} \sim OD_{min} + \frac{(OD_{max} - OD_{min})}{1 + e^{\mu(x_{mid} - time)}} \quad (\text{Eq. 4})$$

404 where  $OD_{min}$  is the minimum population biomass,  $OD_{max}$  is the maximum population biomass,  
 405  $x_{mid}$  is the time to the inflection point, and  $\mu$  quantifies the curve's steepness. The following  
 406 demographic parameters were extracted for each trajectory: the maximum predicted value for  
 407  $OD_{600}$  ( $K$ ; unit:  $OD_{600}$ ); the maximum rate of biomass increase ( $r$ ; unit:  $\text{min}^{-1}$ ); and the maximum  
 408 rate of biomass production (unit:  $OD_{600} \text{ min}^{-1}$ ).

409 **Metabolic Assays.** We measured metabolic rates based on oxygen consumption. The clones  
 410 were revived from the frozen stocks by plating on LB agar. Single colonies were used to  
 411 inoculate 2 mL of DM800 medium, and the cultures were incubated at 37°C with orbital shaking  
 412 for 24 h. The next day, the cells were pelleted by centrifugation, washed with DM0 medium (i.e.,  
 413 DM without added glucose) to remove any residual glucose and extracellular by-products. The  
 414 pellets were resuspended in 2 mL of DM0, and the cultures were then adjusted to  $OD_{600}$  values  
 415 of 0.15, 0.3, and 0.6 and a final volume of 5 mL each using DM0.

416 Oxygen consumption was measured in a temperature-controlled room at 37°C using 4 x 24-  
 417 channel PreSens Sensor Dish Reader (SDR; AS-1 Scientific Wellington, New Zealand), using  
 418 methods adopted from Malerba et al. (31). Before the experiment, the equipment was kept  
 419 overnight in the 37°C room, and each SDR plate was calibrated using air-saturated DM800  
 420 medium (100% air saturation) and DM800 medium containing 2% sodium sulphite (0% air  
 421 saturation). We monitored a total of 192 cultures that included the 2 ancestral and 48 evolved  
 422 clones (including the two 60,000-generation clones from population Ara-3 that were later  
 423 excluded) at each of the three initial cell densities, plus an additional 21 replicates of ancestral  
 424 strain REL606 and 21 blanks without any cells. The additional ancestral replicates meant that  
 425 each 24-well plate included this reference strain at all three cell densities, allowing us to detect  
 426 possible plate-level anomalies; however, we encountered no such problems. The cultures were  
 427 otherwise randomly distributed over two consecutive days of data collection. Each culture was  
 428 carefully placed in a 5-mL vial to avoid creating any air pockets. At least two vials per plate were  
 429 filled with sterile medium that served as blanks. Before starting the trials, all cultures were  
 430 acclimated to 37°C for an hour. We added 0.4  $\mu\text{L}$  of 10% glucose solution to each 5-mL sample  
 431 prior to the start of the assays, which brought the glucose concentration to 8 mg/L (about one-  
 432 third of the concentration in the standard LTEE medium, DM25). Moreover, even the lowest  
 433 initial density ( $OD_{600} = 0.15$ ) is higher than the final density the bacteria reach when they have

434 depleted the glucose in DM25. Thus, the glucose supply was quickly exhausted during these  
435 metabolic assays, with the depletion occurring faster at the higher cell densities. This effect led  
436 to different estimates of metabolic rates across the three cell density treatments; however, the  
437 scaling exponent between cell volume and metabolic rate was unaffected by the treatment (Fig.  
438 2). The assays began after the SDR channels were fully loaded and the samples were well  
439 mixed. The non-consumptive O<sub>2</sub> sensors then monitored the oxygen in each vial every minute  
440 until it was consumed by the bacteria.

441 After the assays ended, the rate of change in oxygen saturation (VO<sub>2</sub>) was quantified from the  
442 linear part of each time-series (Fig. S1). Energy rates were calculated with the following model:

$$VO_2 = \frac{m_a - m_b}{100} V \beta O_2 \quad (\text{Eq. 5})$$

443 where  $m_a$  is the rate of change in each sample (% min<sup>-1</sup>),  $m_b$  is the mean rate of change for the  
444 blanks in each plate (% min<sup>-1</sup>),  $V$  is the water volume (0.005 L), and  $\beta O_2$  is the oxygen capacity  
445 of air-saturated water at 37°C and zero salinity (210 μmol O<sub>2</sub> L<sup>-1</sup>). The rates were then  
446 converted to energy units, assuming a caloric energy of 0.512 J (μmol O<sub>2</sub>)<sup>-1</sup> from Malerba et al.  
447 (31).

448 **Calibration Curves for OD and Cell Density.** In order to express metabolism and productivity  
449 on a *per capita* basis, we performed calibrations to convert oxygen consumption (VO<sub>2</sub>) and  
450 carrying capacity ( $K$ ) from units of OD<sub>600</sub> to units of cells per mL. To this end, we measured cell  
451 densities using two approaches. The first used a Neubauer Improved hemocytometer (Bright-  
452 line double ruled, Pacific Lab) to estimate cell densities for calculating *per capita* respiration  
453 rates. The bacteria were growing, at least briefly, during the respiration measurements, and  
454 therefore these calibrations used growing cultures. Clones were revived from glycerol stocks by  
455 inoculation into 1 mL LB medium and grown overnight. Cells were washed 3 times in 1 X PBS  
456 and then diluted 1000-fold in 3 mL of DM100 medium, where they grew at 37°C with orbital  
457 shaking for 24 h. The next day, the cultures were diluted 20-fold into 200 μL of DM400 medium  
458 in a 96-well microplate. We used DM400 (instead of DM25, DM50, or DM100) so that cell  
459 densities were comparable to those used in the metabolic assays. We immediately measured  
460 an initial OD<sub>600</sub> value for each well using the same ELx808 Incubating Absorbance Microplate  
461 Reader as for the population growth measurements. We then placed the plate in a Thermo  
462 Scientific plate shaker at 37°C and 750 rpm for 2 h. We recorded another set of OD<sub>600</sub> readings,  
463 and then took a 20-μL sample from each well and diluted it to a final concentration of 5%

464 formaldehyde to fix the cells. We returned the plate to the shaker at 37°C. Every hour, we  
465 recorded OD<sub>600</sub> readings and took and fixed 20-μL samples for hemocytometer cell counts until  
466 5 h had elapsed. Three to four replicate cultures were analyzed for each clone, with a blinded  
467 set of clones used for measurements, which were conducted over 20 days. We rarely measured  
468 replicates from the same clone on a given day. Fixed cells were mixed by pipetting up and  
469 down, and we transferred 10 μL into the Neubauer chamber. We used a light microscope to  
470 count the cells. We ran a linear regression to convert OD values to cell densities for each  
471 sample, which we then used to convert oxygen consumption to *per capita* metabolic rates.

472 Maximum OD values typically occurred in our population-growth assays when the cells depleted  
473 the glucose and began to enter stationary phase. Bacterial cells are smaller, on average, in  
474 stationary phase than while growing, including in the LTEE populations (21). Therefore, the  
475 calibrations described above could not be used to estimate maximum cell density ( $Max_{cells}$ ).  
476 Instead, we performed additional calibrations using cultures grown to stationary phase at the  
477 same glucose concentrations as in the growth assays (DM25, DM50, and DM100). We  
478 estimated stationary-phase densities at 24 h by plating cells on MG agar. Clones were revived  
479 from frozen stocks and grown in DM25. Aliquots of these cultures were distributed at random  
480 over multiple 96-well microplates to minimize position effects. After 24 h at 37°C on a plate  
481 shaker, each culture was diluted 100-fold in DM25, DM50, and DM100 (2 μL of culture in 200 μL  
482 of fresh medium) and incubated again for 24 h on the shaker. These cultures were diluted  
483 10,000-fold and spread on MG agar plates, and colonies were counted after incubating the  
484 plates for 24 h. We used these counts to calibrate stationary-phase cell densities based on  
485 colony-forming units at 24 h ( $N_{CFU}$ ) and cell densities inferred from OD values and  
486 hemocytometer counts of growing cells ( $N_{OD}$ ), which yielded the following equation (Fig. S2):  
487  $\log_{10}[N_{CFU}] = 0.92 \times \log_{10}[N_{OD}] + 1.35$ . We then used this equation to estimate  $Max_{cells}$  as the cell  
488 density corresponding to the maximum OD reading ( $OD_{max}$ ) from each growth curve. The  
489 60,000-generation sample from population Ara+3 appeared to be an outlier when calibrating the  
490 relation between cell numbers based on OD and CFU values (Fig. S2). (Note: This outlier is not  
491 the Ara-3 sample that was excluded from all of our analyses because the cells can grow on  
492 citrate). We therefore recalculated all the scaling exponents in this work while excluding this  
493 outlier, but none of the values changed substantively (Table S2).

494 **Cell Size Measurements.** We measured the mean cell volume for each clone in stationary  
495 phase using the side-scatter of a flow cytometer (Flow-Core, BD LSR II, BD Biosciences, San  
496 Jose, CA); beads of four diameters (0.2, 0.5, 1, and 2 μm, Invitrogen by Thermo Fisher

497 Scientific) served as standards. The clones were revived from frozen stocks and grown in DM25  
498 at 37°C with orbital shaking for 24 h. The next day, these acclimated cells were diluted 100-fold  
499 in fresh DM25 medium in 96-well microplates. We had four replicates per clone, and the clones  
500 were randomly placed across four plates. The plates were incubated at 37°C and 750 rpm for  
501 another 24 h, at which time samples were taken and used for flow cytometry. The cell volumes  
502 we obtained using this approach are very similar to those previously obtained using microscopy  
503 and electronic size-based particle counts (21).

504 **Statistical Analyses.** Metabolic rates and growth models were calculated using R (49) and the  
505 packages nlme (50), lme4 (51), and plyr (52) for model fitting. ANCOVA and multiple regression  
506 models were performed using Systat to examine the scaling relations between average log-  
507 transformed cell volume and the various log-transformed metabolic and population dynamics  
508 metrics, respectively; initial cell density (in the case of metabolism) and glucose level (in the  
509 case of population dynamics) were additional covariates or fixed factors. In all cases, we  
510 calculated mean values across technical replicates for a given clone, and we then averaged the  
511 values for the two clones sampled from each LTEE population at either 10,000 or 60,000  
512 generations.

513 **Data Availability.** The data used in this study are deposited at the Dryad Digital Repository  
514 (doi: pending).

515 **ACKNOWLEDGMENTS.** We thank Craig White and Nkrumah Grant for valuable discussions,  
516 and two anonymous reviewers for constructive suggestions. This work was supported, in part,  
517 by the US National Science Foundation (grant DEB-1951307) to R.E.L. and an Australian  
518 Research Council Future Fellowship (grant FT170100441) to M.J.M.

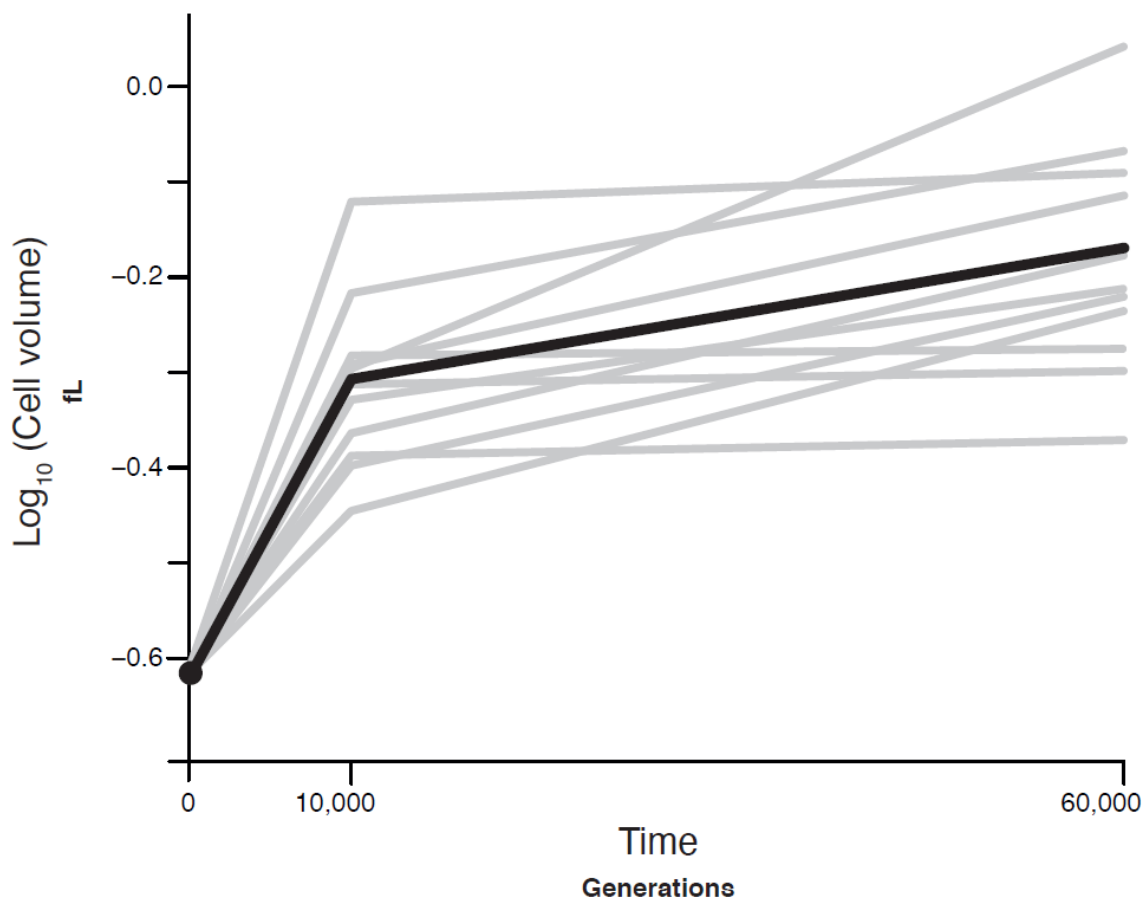
519

520 **References**

- 521 1. I. A. Hatton *et al.*, The predator-prey power law: Biomass scaling across terrestrial and  
522 aquatic biomes. *Science* **349**, aac6284 (2015).
- 523 2. M. E. Malerba, D. J. Marshall, Size-abundance rules? Evolution changes scaling  
524 relationships between size, metabolism and demography. *Ecol. Lett.* **22**, 1407-1416 (2019).
- 525 3. N. J. B. Isaac, D. Storch, C. Carbone, The paradox of energy equivalence. *Glob. Ecol.*  
526 *Biogeog.* **22**, 1-5 (2013).
- 527 4. I. A. Hatton, A. P. Dobson, D. Storch, E. D. Galbraith, M. Loreau, Linking scaling laws  
528 across eukaryotes. *Proc. Natl. Acad. Sci., USA* **116**, 21616-21622 (2019).
- 529 5. J. Damuth, Population density and body size in mammals. *Nature* **290**, 699-700 (1981).
- 530 6. V. M. Savage, J. F. Gillooly, J. H. Brown, G. B. West, E. L. Charnov, Effects of body size  
531 and temperature on population growth. *Am. Nat.* **163**, 429-441 (2004).
- 532 7. J. Forster, A. G. Hirst, D. Atkinson, Warming-induced reductions in body size are greater in  
533 aquatic than terrestrial species. *Proc. Natl. Acad. Sci., USA* **109**, 19310-19314 (2012).
- 534 8. A. Audzijonyte *et al.*, Fish body sizes change with temperature but not all species shrink  
535 with warming. *Nat. Ecol. Evol.* **4**, 809-814 (2020).
- 536 9. J. L. Gardner, A. Peters, M. R. Kearney, L. Joseph, R. Heinsohn, Declining body size: a  
537 third universal response to warming? *Trends Ecol. Evol.* **26**, 285-291 (2011).
- 538 10. A. Audzijonyte, A. Kuparinen, R. Gorton, E. A. Fulton, Ecological consequences of body  
539 size decline in harvested fish species: positive feedback loops in trophic interactions amplify  
540 human impact. *Biol. Lett.* **9**, 20121103 (2013).
- 541 11. J. R. Bernhardt, J. M. Sunday, M. I. O'Connor, Metabolic theory and the temperature-size  
542 rule explain the temperature dependence of population carrying capacity. *Am. Nat.* **192**,  
543 687-697 (2018).
- 544 12. N. J. B. Isaac, C. Carbone, B. McGill, in *Metabolic Ecology: A Scaling Approach* (eds R.  
545 Sibly, J. H. Brown, A. Kodric-Brown) 77-85. Wiley-Blackwell: Oxford, UK (2012).
- 546 13. A. Hayward, J. Kolasa, J. R. Stone, The scale-dependence of population density–body  
547 mass allometry: Statistical artefact or biological mechanism? *Ecol. Comp.* **7**, 115-124  
548 (2010).
- 549 14. C. P. Kempes, S. Dutkiewicz, M. J. Follows, Growth, metabolic partitioning, and the size of  
550 microorganisms. *Proc. Natl. Acad. Sci., USA* **109**, 495-500 (2012).
- 551 15. R. E. Lenski, M. R. Rose, S. C. Simpson, S. C. Tadler, Long-term experimental evolution in  
552 *Escherichia coli*. I. Adaptation and divergence during 2,000 generations. *Am. Nat.* **138**,  
553 1315-1341 (1991).
- 554 16. M. J. Wisser, N. Ribeck, R. E. Lenski, Long-term dynamics of adaptation in asexual  
555 populations. *Science* **342**, 1364-1367 (2013).
- 556 17. O. Tenaillon *et al.*, Tempo and mode of genome evolution in a 50,000-generation  
557 experiment. *Nature* **536**, 165-170 (2016).
- 558 18. B. H. Good, M. J. McDonald, J. E. Barrick, R. E. Lenski, M. M. Desai, The dynamics of  
559 molecular evolution over 60,000 generations. *Nature* **551**, 45-50 (2017).
- 560 19. R. E. Lenski, M. Travisano, Dynamics of adaptation and diversification: a 10,000-generation  
561 experiment with bacterial populations. *Proc. Natl. Acad. Sci., USA* **91**, 6808-6814 (1994).
- 562 20. R. Gallet *et al.*, The evolution of bacterial cell size: the internal diffusion-constraint  
563 hypothesis. *ISME J.* **11**, 1559-1568 (2017).
- 564 21. N. A. Grant, A. Abdel Magid, J. Franklin, Y. Dufour, R. E. Lenski, Changes in cell size and  
565 shape during 50,000 generations of experimental evolution with *Escherichia coli*. *J.*  
566 *Bacteriol.* **203**, e00469-20 (2020).

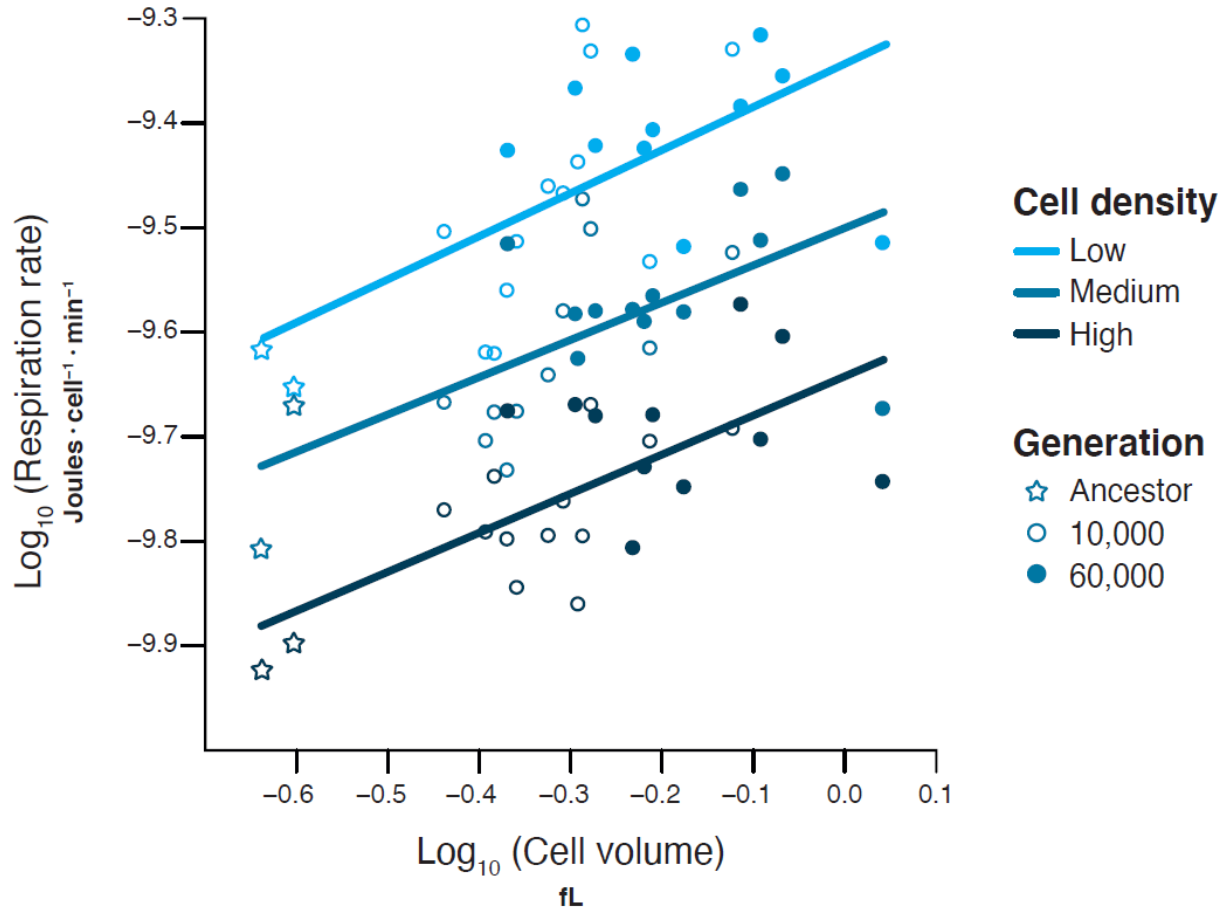
- 567 22. M. Travisano, J. A. Mongold, A. F. Bennett, R. E. Lenski, Experimental tests of the roles of  
568 adaptation, chance, and history in evolution. *Science* **267**, 87-90 (1995).
- 569 23. M. Novak *et al.*, Experimental tests for an evolutionary trade-off between growth rate and  
570 yield in *E. coli*. *Am. Nat.* **168**, 242-251 (2006).
- 571 24. M. T. Wortel, E. Noor, M. Ferris, F. J. Bruggeman, W. Liebermeister, Metabolic enzyme  
572 cost explains variable trade-offs between microbial growth rate and yield. *PLoS Comp. Biol.*  
573 **14**, 21 (2018).
- 574 25. Z. D. Blount, C. Z. Borland, R. E. Lenski, Historical contingency and the evolution of a key  
575 innovation in an experimental population of *Escherichia coli*. *Proc. Natl. Acad. Sci., USA*  
576 **105**, 7899-7906 (2008).
- 577 26. J. P. DeLong, J. G. Okie, M. E. Moses, R. M. Sibly, J. H. Brown, Shifts in metabolic scaling,  
578 production, and efficiency across major evolutionary transitions of life. *Proc. Natl. Acad.*  
579 *Sci., USA* **107**, 12941-12945 (2010).
- 580 27. E. Litchman, in *Metabolic Ecology: A Scaling Approach* (eds R. Sibly, J. H. Brown, & A.  
581 Kodric-Brown) 154-164 (2012).
- 582 28. D. M. Perkins *et al.*, Energetic equivalence underpins the size structure of tree and  
583 phytoplankton communities. *Nat. Comm.* **10**, 1-8 (2019).
- 584 29. F. C. García *et al.*, The allometry of the smallest: superlinear scaling of microbial metabolic  
585 rates in the Atlantic Ocean. *ISME J.* **10**, 1029-1036 (2016).
- 586 30. M. E. Malerba, C. R. White, D. J. Marshall, Phytoplankton size-scaling of net-energy flux  
587 across light and biomass gradients. *Ecology* **98**, 3106-3115 (2017).
- 588 31. M. E. Malerba, C. R. White, D. J. Marshall, Eco-energetic consequences of evolutionary  
589 shifts in body size. *Ecol. Lett.* **21**, 54-62 (2018).
- 590 32. K. J. Niklas, *Plant Allometry: The Scaling of Form and Process*. Chicago: Univ. Chicago  
591 Press (2004).
- 592 33. J. Kozłowski, M. Konarzewski, A. T. Gawelczyk, Cell size as a link between noncoding DNA  
593 and metabolic rate scaling. *Proc. Natl. Acad. Sci., USA* **100**, 14080-14085 (2003).
- 594 34. T. F. Cooper, D. E. Rozen, and R. E. Lenski, Parallel changes in gene expression after  
595 20,000 generations of evolution in *Escherichia coli*. *Proc. Natl. Acad. Sci., USA* **100**, 1072-  
596 1077 (2003).
- 597 35. N. Philippe, E. Crozat, R. E. Lenski, D. Schneider, Evolution of global regulatory networks  
598 during a long-term experiment with *Escherichia coli*. *Bioessays* **29**, 846-860 (2007).
- 599 36. J. S. Favate, S. Liang, S. S. Yadavalli, P. Shah, The landscape of transcriptional and  
600 translational changes over 22 years of bacterial adaptation. *bioRxiv*  
601 doi:10.1101/2021.01.12.426406 (2021).
- 602 37. R. Maddamsetti *et al.*, Core genes evolve rapidly in the long-term evolution experiment with  
603 *Escherichia coli*. *Genome Biol. Evol.* **9**, 1072-1083 (2017).
- 604 38. J. A. Mongold, R. E. Lenski, Experimental rejection of a nonadaptive explanation for  
605 increased cell size in *Escherichia coli*. *J. Bacteriol.* **178**, 5333-5334 (1996).
- 606 39. M. Szenk, K. A. Dill, A. M. R. de Graff, Why do fast-growing bacteria enter overflow  
607 metabolism? Testing the membrane real estate hypothesis. *Cell Syst.* **5**, 95-104 (2017).
- 608 40. J. H. Brown, J. F. Gillooly, A. P. Allen, V. M. Savage, G. B. West, Toward a metabolic  
609 theory of ecology. *Ecology* **85**, 1771-1789 (2004).
- 610 41. M. Lynch, G. K. Marinov, The bioenergetic costs of a gene. *Proc. Natl. Acad. Sci., USA*  
611 **112**, 15690-15695 (2015).
- 612 42. A. H. Stouthamer, C. W. Bettenhausen, Continuous culture study of an APTase-negative  
613 mutant of *Escherichia coli*. *Arch. Microbiol.* **113**, 185-189 (1977).

- 614 43. K. J. Niklas, S. T. Hammond, Biophysical effects on the scaling of plant growth, form, and  
615 ecology. *Integ. Comp. Biol.* **59**, 1312-1323 (2019).
- 616 44. C. B. Turner, B. D. Wade, J. R. Meyer, B. A. Sommerfeld, R. E. Lenski, Evolution of  
617 organismal stoichiometry in a long-term experiment with *Escherichia coli*. *Roy. Soc. Open*  
618 *Sci.* **4**, 170497-170497 (2017).
- 619 45. M. E. Malerba, G. Ghedini, D. J. Marshall, Genome size affects fitness in the eukaryotic  
620 alga *Dunaliella tertiolecta*. *Curr. Biol.* (2020).
- 621 46. R. E. Lenski, Experimental studies of pleiotropy and epistasis in *Escherichia coli*. I.  
622 Variation in competitive fitness among mutants resistant to virus T4. *Evolution* **42**, 425-432  
623 (1988).
- 624 47. M. Izutsu, D. M. Lake, Z. W. D. Matson, J. P. Dodson, R. E. Lenski, Effects of periodic  
625 bottlenecks on the dynamics of adaptive evolution in microbial populations. *bioRxiv*  
626 2021.12.29.474457 (2021).
- 627 48. M. E. Malerba, M. M. Palacios, D. J. Marshall, Do larger individuals cope with resource  
628 fluctuations better? An artificial selection approach. *Proc. R. Soc. London B* **285**, 1-9  
629 (2018).
- 630 49. R Core Team, R: A Language and Environment for Statistical Computing. R Foundation for  
631 Statistical Computing, Vienna, Austria (2019).
- 632 50. J. Pinheiro, D. Bates, S. DebRoy, D. Sarkar, R Core Team, nlme: linear and nonlinear  
633 mixed effects models. R package version 3.1-128 (2016).
- 634 51. D. Bates, M. Mächler, B. Bolker, S. Walker, Fitting linear mixed-effects models using lme4.  
635 *J. Stat. Softw.* **67**, 1-48 (2015).
- 636 52. H. Wickham, The split-apply-combine strategy for data analysis. *J. Stat. Softw.* **40**, 1-29  
637 (2011).
- 638
- 639



642  
643 **Fig. 1.** Trajectories of cell size in *E. coli* populations across 60,000 generations of evolution. The  
644 black line shows the mean trajectory of all populations; grey lines show the 12 independent  
645 populations. The 60,000-generation sample from one population is excluded, because it evolved  
646 the ability to use an additional resource not available to the other bacteria (see Materials and  
647 Methods).

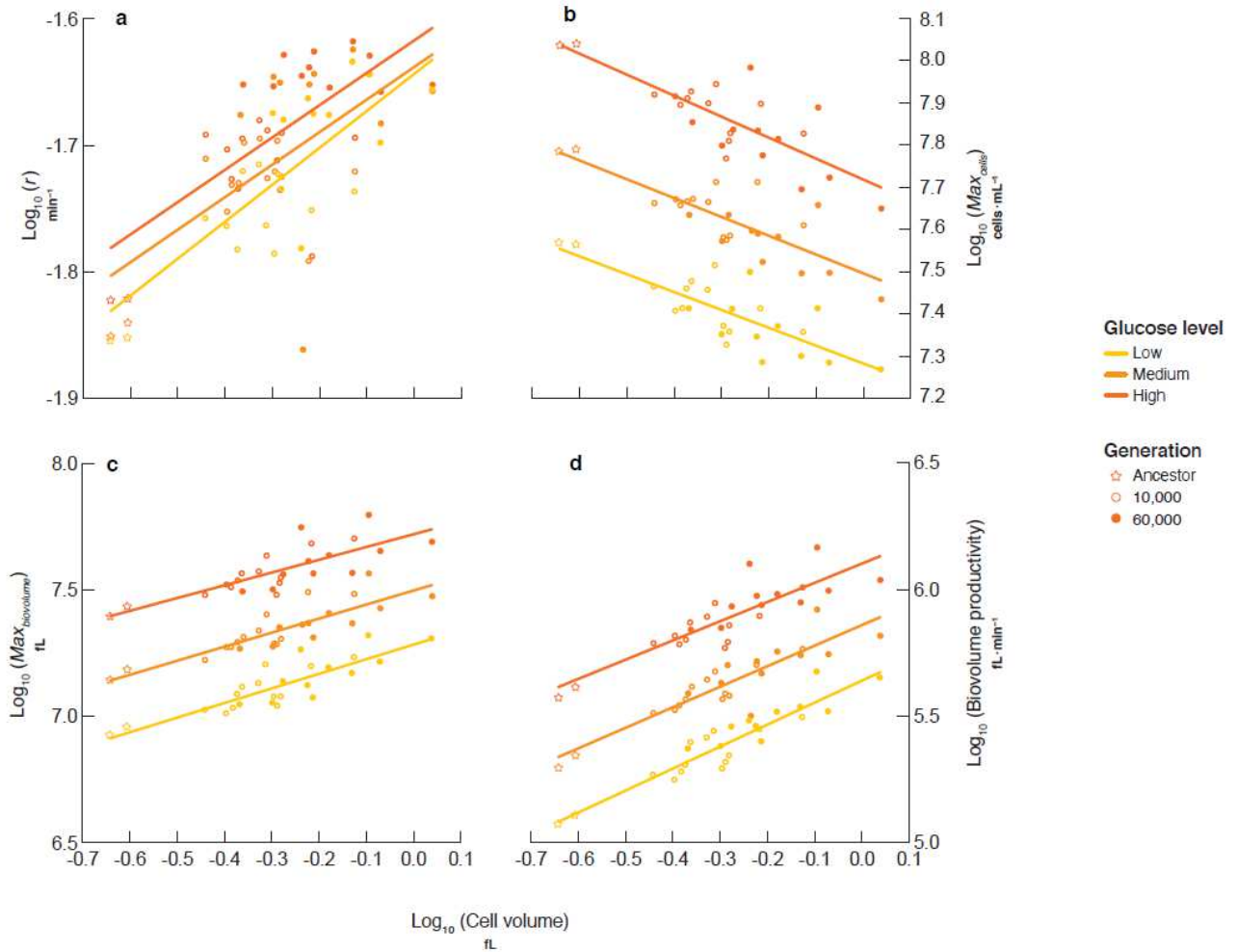
648



649

650 **Fig. 2.** Scaling relation between average cell volume and *per capita* metabolic rate. The relation  
 651 was examined across three different total biomasses, achieved by varying the initial cell density  
 652 (shown by different colors). The limiting glucose concentration was the same for all three  
 653 treatments; the glucose was thus depleted faster at the higher cell densities, leading to lower  
 654 *per capita* metabolic rates. Each point shows the mean value for a sample at the generation  
 655 indicated by the different symbols. The resulting estimate of the metabolic scaling exponent,  $B$ ,  
 656 is 0.38 and statistically indistinguishable across densities.

657



658

659 **Fig. 3.** Scaling relations between average cell volume and a) intrinsic rate of population growth;  
 660 b) maximum population density in terms of cell number; c) maximum population density in terms  
 661 of total biovolume; and d) maximum rate of biovolume productivity. Different colors represent  
 662 different glucose levels (low: DM25; medium: DM50; high: DM100). The low level, DM25, is the  
 663 same medium used in the LTEE. Each point shows the mean value for a sample from the  
 664 generation indicated by the different symbols.

665

666

667 **Table 1. Summary of predicted and observed scaling of population parameters based on metabolic scaling theory.** We estimated the  
668 metabolic scaling exponent,  $B$ , as 0.38 (Fig. 2). We show predictions (including confidence intervals in parentheses) based on the standard  
669 theory, whereby production costs are assumed to scale perfectly with size ( $C = 1$ ); when production costs are assumed to be size invariant ( $C =$   
670  $0$ ); and when production costs scale weakly with size ( $C = 0.11$ ). The  $C$  value of 0.11 was calculated based on the scaling observed for the  
671 intrinsic rate of increase,  $r$ .

Parameter	Definition	General theory	Prediction if $C = 1$	Prediction if $C = 0$	Prediction if $C = 0.11$	Observed scaling
$r$	Intrinsic rate of increase	$M^{B-C}$	-0.62 (-0.73:-0.51)	0.38 (0.27:0.49)	0.27 (0.16:0.38)	0.27 (0.20:0.34)
$Max_{cells}$	Maximum cell density	$M^{-B}$	-0.38 (-0.49:-0.27)	-0.38 (-0.49:-0.27)	-0.38 (-0.49:-0.27)	-0.45 (-0.54:-0.37)
$Max_{biovolume}$	Maximum population biovolume	$M^{1-B}$	0.62 (0.51:0.73)	0.62 (0.51:0.73)	0.62 (0.51:0.73)	0.55 (0.46:0.63)
$Biovolume\ productivity$	Maximum productivity	$M^{(1-B)} \times M^{(B-C)} = M^{1-C}$	0	1	0.89	0.81 (0.72:0.91)

672

673

674